Journal of The Electrochemical Society

Pseudocapacitive Charge Storage in Electrochromic Transition-Metal Oxide Thin Films

To cite this article: Dongmei Dong *et al* 2022 *J. Electrochem. Soc.* **169** 080511

Pseudocapacitive Charge Storage in Electrochromic Transition-Metal Oxide Thin Films

Journal:	*Journal of The Electrochemical Society*
Manuscript ID	JES-106453.R1
Manuscript Type:	Research Paper
Date Submitted by the Author:	05-Apr-2022
Complete List of Authors:	Dong, Dongmei; Florida International University, Electrical and computing Benhaddouch, Tinsley ; Florida International University, Department of Electrical and Computer Engineering Metler, Christopher; Florida International University, Department of Marine Biology Marcial, John; Florida International University Zhao, Yaoli; University at Buffalo School of Engineering and Applied Sciences, Venkadesh, Vagheeswari; Florida International University Thundat, Thomas; University at Buffalo - The State University of New York, Chemical and Biological Engineering; Prof. Bhansali, Shekhar; Florida International University, Electrical and computer engineering
Keywords:	Films, Optical films, Sputtering, Batteries – Li-ion

Pseudocapacitive Charge Storage in Electrochromic Transition-Metal Oxide Thin Films

Dongmei Dong, Tinsley Elizabeth Benhaddouch,[1,*] Christopher Lloyd Metler,[2] John Marcial,[1] Yaoli Zhao,[3] Vagheeswari Venkadesh,[4] Thomas Thundat,[3,**] and Shekhar Bhansali[1,*]

[a] Department of Electrical and Computer Engineering, Florida International University, Miami, Florida, USA
[b] Department of Marine Biology, Florida International University, Miami, USA
[c] Department of Chemical and Biological Engineering, State University of New York at Buffalo, New York, USA
[d] Department of Earth and Environment, Florida International University, Miami, USA

*Electrochemical Society Student Member.
**Electrochemical Society Member.

[z]E-mail: ddong@fiu.edu

Abstract

Electrochromic pseudocapacitive transition-metal oxide materials, such as tungsten oxide, which combine fast response, high energy density, and optical effects, can play a significant role as energy storage materials. Here we investigate the electrochemical kinetics of thin films of tungsten oxide, which turn transparent to sky-blue color in the lithiated state due to the reduction of W^{6+} to W^{5+}. We investigated the charge density, charge transfer, ion diffusion, and interfacial behavior upon Li^+ insertion/de-insertion in WO_3. The electrochromic thin film's pseudocapacitive and electrical double layer mechanism was differentiated based on the power-law. Faradaic diffusion-controlled process dominates over the surface capacitive behavior at scan rates below 40 mV/s. These films exhibit an areal charge density of around 100 mC/cm2 and a capacitance of 80 mF/cm2, superior to most comparable electrochromic materials and supercapacitors. This work combines electrochromics and energy storage properties and provides a fundamental understanding of pseudocapacitive and electrochromic mechanisms in WO_3.

Introduction

In recent years, pseudocapacitive materials have attracted attention for applications in high power density Li-ion storage systems[1]. Because of their fast charge-discharge rates and energy-dense electrochemical faradaic charge storage behavior, these materials have the potential to enable diverse applications. Transition metal oxides are of growing interest among many materials systems due to their multiple valence states, allowing faster faradaic reactions and higher energy density.

It has been widely recognized that electrochemical kinetics of pseudocapacitive materials can support tunable electrochemical performance and increased charge storage rates for electrochemical energy storage systems. However, charge storage mechanisms in pseudocapacitive materials and their electrochemical responses are still poorly understood and are the focus of active investigations.

Electrochromic (EC) materials show reversible optical changes depending on the extent of electrochemical redox reactions under externally applied potentials[2]. Currently, EC properties of transition metal oxides are investigated for diverse applications ranging from rearview mirrors, smart windows, displays, and wearable electronics[3] to bifunctional supercapacitors[4-6] and real-time indicators[7,8]. Pseudocapacitive EC materials show promise as multifunctional/smart electronic systems[9] because of their ability to provide visual recognition of the degree of charge/discharge status. However, such applications require understanding EC films' electrochemical charge-transfer kinetics, diffusion kinetics, and solid-electrolyte interface behavior.

Tungsten oxide (WO_3), an EC transition-metal oxide, exhibits excellent chemical and electrochemical performance and shows sky-blue color in the lithiated state due to the reduction of W^{6+} to W^{5+}. The color intensity, correlated to the amounts of charges introduced into the material, can be modulated gradually by the applied potential presented in our previous work[10]. Therefore, coupling these materials' EC and energy storage properties opens new paths for many practical applications of EC materials. In addition, such coupling will strengthen the fundamental understanding of energy storage mechanisms for industrial-scale applications, such as capacitors, batteries, etc.

WO_3 is the preferred electrode material for multifunctional EC pseudo capacitor development due to its rapid electrochemical charge storage/release ability. However, improving the system performance will require separating the different processes (diffusion-controlled and surface capacitive) involved and understanding their evolution with electrochemical kinetics. This area, which remains largely unexplored, is the focus of the current paper.

In this work, methods based on electrochemical kinetics were employed to investigate electrochromism, charge transfer, and interfacial properties of WO_3. Simultaneous electrochemical energy storage and EC color switching of WO_3 were studied at various applied potentials under electrochemical control. Besides using cyclic voltammetry (CV) and multi-step chronoamperometry (MSCA), electrochemical impedance spectroscopy (EIS) was also carried out to investigate the interfacial effects. The battery-like behavior and electrical double layer contribution were quantitively separated in the dynamic electrochemical process, giving a better insight into the EC mechanism and pseudocapacitive behavior. This article aims to broaden the applications of EC materials and provide new insights for designing energy storage devices.

Experimental

Deposition of WO_3 thin solid films

The WO_3 thin solid films were fabricated with a reactive direct current magnetron sputtering technique from a circular tungsten metal target (purity: 99.95%, diameter: 60 mm, thickness: 3 mm). The deposition atmosphere was a mixture of O_2 (purity: 99.99%) and Ar (purity: 99.99%). The gas composition ratio of Ar to O_2 was 5:2, resulting in a total pressure of 1.7 Pa. The power used was 250 W. The substrate is commercial transparent indium tin oxide (ITO, square resistance R_s: 30 Ω; Thickness: 100 nm). The WO_3 film thickness was measured to be around 480 nm.

Characterization

The electrochemical measurements, including the CV, MSCA, and EIS, were carried out in a three-electrode system using an electrochemical workstation (Metrohm, PGSTAT30 potentiostat). The lithium perchlorate $LiClO_4$ powder (purity: 99^+%, Thermo Scientific) and propylene carbonate (PC) liquid (purity: 99.5%, Thermo Scientific) were used to prepare the electrolyte 1M $LiClO_4$-PC. The working electrode was a commercial Glass/ITO on which thin solid films of WO_3 (thickness around 480 nm) were deposited by vacuum deposition. The counter and reference electrodes were platinum wire and Ag/AgCl, respectively. The potentials reported in this work are referenced against Ag/AgCl. We used 1 M PC-$LiClO_4$ as the electrolyte in these experiments. In the CV scans, an gradually enlarging potential window is applied to get the optimal voltage range where the redox peaks are fully completed; Meanwhile, the sweep rate remains constant at 100 mV/s. To study the effect of the scan rate, the potential is kept at the optimal range [-1.3V, 1.4V]; A continuously decreasing scan rate from 200 mV/s to 50 mV/s is investigated. The charge Q is also recorded as the 2nd signal for each scan. In the MSCA experiments, various potential steps and duration times are applied. In process I, the potentials increases from $\pm$0.3V to $\pm$1.2V, and the duration time for each step is 30s; In process II, an extended duration time 60s is applied to allow for the complete redox reactions; In process III, the current response in function of the voltage and duration is double confirmed. The alternating current impedance spectra were collected in the frequency range *f* starting from 100 kHz to 0.1 Hz, in 3 consequent processes of coloration at 8 voltages from -0.1 to -0.45V, bleaching at 4 voltages from +0.1 to +0.25V and re-coloration at -0.30V/re-bleaching at +0.30V. The data were presented in the Nyquist plot. The EIS modeling was carried out with the software ZView. The optical properties of the thin films were determined *ex-situ* by using an ultraviolet-visible (UV-Vis) spectrophotometer at colored/bleached states at different voltages (Thermo Scientific, Evolution 220). Optical profilometry measurements were carried out using a three-dimensional optical profilometer (Model Profilm3D). The optical profilometer was housed in a vibration-resistant table to eliminate ambient building vibrations. The raw data were acquired and then processed using the "ProfilmOnline" software.

Results and discussion

Cyclic Voltammetry (CV)

Cyclic voltammetry studies showed that the mole fraction of inserted Li^+ increased with film structure, applied potential, and the reaction time until saturation[11]. The charge storage in the WO_3 electrode is significantly dependent on the electrochemical potential (window between -1.3 to 1.43 V) and sweep rates (200 to 50 mV/s). Charge density Q (mC/cm^2) can be calculated by the integral of current density j (mA/cm^2) to the applied time *(t)* using $Q=\int_{t1}^{t2} j dt$. For CV, the formula can be re-written, including the scan rate v (mV/s) as $\int_{V_1}^{V_2} j \frac{dV}{v}$. Therefore, enlarging the potential window while decreasing the sweep rate (v) can increase the total charge stored in the system. This relationship also shows that the maximum storage capacity cannot be obtained at the given potential or v value, owing to the kinetic limitations imposed by the Li^+ diffusion process. The evolution in the CV shapes shows the voltage/rate-limiting kinetics for the charge storage process. As shown in Fig.1a, the CV is in a fusiform-like shape at a small potential window. As potential increases, the CV becomes more rotund near the positive end until the complete oxidation reaction is obtained, as shown by a triangle-like shape. The broad peaks observed at various scan rates in the CV curves indicate a typical intercalation pseudocapacitive behavior of WO_3[12,13]. In the coloration part of the CV loop, the current increases until the potential is reversed. As shown in Fig.1a & 1c, this continuously-growing near-linear current originates from the Faradic reaction of reducing W^{6+} to W^{5+}. These results demonstrate that optimizing the potential window range and v reduction within a certain region is crucial for enhancing the total stored charges and the EC coloration/bleaching behavior.

Multi-Step Chronoamperometry (MSCA)

In addition to CV analysis, electrochemical dynamics were also studied as functions of applied potential steps and different duration time in the MSCA, as shown in Fig.1e as regions I, II, and III. In Fig.1e, the time duration for bleaching/coloration is 30s in region I, 60s in region II, and 90s in region III. The potential steps in these regions were changed from ± 0.3 to ± 1.2 V, as shown in Fig.1e. For EC cathodic WO_3 electrode, the upper curve represents bleaching while the lower curve shows coloration for each cycle. The evolution of charge density Q is investigated by integrating the current density j, as specified at each step of MSCA. Firstly, in general, both j and Q increase with the potential and transient time except the every 1st MSCA step in the regions I to III. The abrupt increase comes from the prior accumulative process of the charges. Secondly, the MSCA curves for bleaching are sharper overall than the coloration process, indicating a faster bleaching response time than that for coloration. It also suggests an asymmetrical feature of the Li^+ extraction and insertion process. It is smoother and quicker for Li^+ to leave WO_3 (de-insertion) but more difficult and slower to get into WO_3 (insertion). After the positive voltage is applied, WO_3 rapidly "pushes" the inserted Li^+ ions out of it. This repelling behavior is very interesting and may account for the self-bleaching and memory effect, which are not fully understood in electrochromics at present. The potential vs. average current density is also plotted to interpret this asymmetric process more. As shown in Fig.1f, the shape/slope is quite different for the coloration and bleaching. The sharper slope in the bleaching response seems to indicate that the film is less conductive caused by Li^+ de-insertion. In the region I of MSCA, as potential is increased, the duration time of 30 s is not enough for a complete coloration reaction. However, the j ramps down rapidly and approaches zero after completing the oxidation reaction during bleaching.

Interestingly, this fast response of Li^+ extraction for bleaching is always accompanied by less than 100% reversibility of charge exchange. For instance, the inserted charge of 33.7 mC/cm^2 is not fully extracted by the following opposite potential corresponding to the extracted charge of 24 mC/cm^2 occurring from 460 to 520 s. The charge inserted and extracted integrated over 900s is 16.1 mC/cm^2 and 14.3 mC/cm^2, respectively, and the difference originates from the irreversibility of Li^+ insertion. The MSCA results clearly show that WO_3 can flexibly adjust its charge storage level according to the potential applied. Encouragingly, a high charge density approaching 100 mC/cm^2 is achieved here at a very low potential of -0.3 V.

Electrochemistry Impedance (EIS)

To obtain the EIS spectra, we monitored the electrochemical impedance as a frequency (f) function. The f response can be useful for identifying the resistive, capacitive, pseudocapacitive, and other impedance elements within an electrochemical system[14]. There are various ways to represent this data. Firstly, the Nyquist plot shows the real component of the abscissa and the imaginary on the ordinate. As per common practice, the -Z" (Ω/cm^2) *vs.* Z' (Ω/cm^2) is plotted so that the data is in the first quadrant.

On the other hand, the Bode plot shows the absolute value of impedance mod(Z) or phase angle as a function of f. Additionally, equivalent circuit models that fit the data can be obtained using ZView software. In this study, it is most appropriate to analyze the EC WO_3 thin solid films using Nyquist plots and equivalent circuit models. Fig. 2a-c shows the Nyquist plots obtained for EC WO_3 thin solid films for coloring, bleaching, and comparisons of re-colored and re-bleached, respectively. Analyzing the data using ZView, we obtain equivalent circuit models for each separate process of coloring the

EC WO_3 thin solid films. The equivalent circuit models used to fit the coloring process's EIS data are embedded in Fig. 2a. Since the models differ in *f* response, components, and configuration, the circuit models used for coloration cannot explain the bleaching process. As seen in Fig. 2, the EIS spectra in bleaching are composed of several processes, which are more complex than the coloration curves, including the charge-transfer semicircle and diffusion tail. This also suggests an asymmetric feature of Li insertion and de-insertion. Table I lists values for each circuit component for the various applied voltages during the experiments. The Semicircle in the higher frequency region followed by a nearly linear component in the lower frequency region is indicative of a mixed kinetic and charge transfer control due to the combination of kinetic and diffusion processes. This makes fitting the components precisely very challenging but using the X^2 (chi-squared fitting parameter), we were able to fit an equivalent circuit with low error for each individual parameter value selected, as listed in Table 1. R_e refers to the Ohmic resistance of the electrolyte and the electrode. The charge transfer resistance parameter R_{ct} is of primary interest for this work and is discussed in detail. CPE-T and CPE-P are components of the Constant Phases Element added to account for the distorted Semicircle. CPE-T relates to the pseudocapacitance and homogeneity of the surface, and CPE-P relates to the depressed Semicircle and the roughness/heterogeneity of the surface. W_o-R, W_o-P, and W_o-T are values related to the Warburg impedance element, where R relates to the "real" impedance, P is the parameter corresponding to the slope between complex and real impedance, and T is the parameter relating to the thickness of the diffusion layer. Lastly, the Chi-squared values represent the error of the equivalent circuit model fit to the actual data, which shows our model is a good approximation to the data. From the parameters used for fitting the EIS data, it is clear that the charge transfer resistance R_{ct} decreases during coloration, but increases during bleaching, and this trend is enhanced as the potential is increased. The interfacial kinetics is favorable for Li^+ insertion. After applying -0.3V, the R_{ct} drops down to 43.28 Ω, which drives the Li^+ into the WO_3 electrode, but bounces back to 193.3 Ω at +0.25 V, corresponding to a fully bleached state.

In detail, the Nyquist plots of the coloring process for the various applied voltages are demonstrated in panel a. Two highly characteristic and distinct regions are evident. The 1^{st} region is the semi-circular region starting at the highest *f* near the origin, primarily associated with the charge transfer resistance R_{ct}. In general, the resistance is approximately the diameter of the Semicircle. The 2nd region increases linearly at approximately a 45-degree angle, known as Warburg diffusion. The charge transfer resistance region remains relatively constant during the coloration, while the Warburg diffusion region varies with applied potential. Inset shows that the Warburg impedance associated with the diffusion resistance varies greatly and differs from the charge transfer resistance. The low *f* region is further investigated to compare the experimentally obtained Warburg coefficients to determine the *f* that is more favorable for ion diffusion. The Warburg factor, σ, is inversely proportional to the diffusion coefficient of the electrolyte ions, and it has a linear relationship with Z', where $Z' = R_e + R_{ct} + \sigma f^{-1/2}$[15,16]. Here, R_e and R_{ct} are the equivalent resistance and the charge transfer resistance. When the potential increases from 0.1 to 0.45 V, the slope decreases from 27 to 7 for σ, indicating an increased diffusion coefficient. The Warburg region for Li^+ insertion for coloration changes drastically from -0.1 to -0.3 V. When the potential goes beyond -0.3 V, the diffusion coefficient gradually stabilizes. This suggests that the available active sites are becoming less and less and are slowly getting saturated.

The following process of the WO_3 thin solid film is represented in Fig. 2c. As discussed earlier, we can see a semi-circular region, though it deviates from a perfect semicircle during the coloration process. Additionally, as the WO_3 becomes more bleached, the charge transfer resistance region becomes less pronounced. The charge transfer region is almost nonexistent when the film is fully bleached. The bleaching process's Warburg region is drastically different from that of the coloration process.

Finally, Fig. 2d shows the comparison between the third Nyquist plots of the re-colored WO_3 to that of the re-bleached. It clearly shows that the re-colored and re-bleached *f* responses follow a similar response pattern as the original coloring and bleaching processes. This can be explained due to the repeatability of the charge transfer and diffusion process in cycling.

Table I. EIS fitted parameters of WO_3 at colored/bleached states.

Parameter	Colored/V			Bleached/V				Re-colored/V
	-0.15	-0.20	-0.45	+0.10	+0.15	+0.20	+0.25	-0.30
R_e (Ω)	9.06E-07	1.09E-06	2.29E-06	0.91	5.90E-06	4.35E-07	1.44E-06	0.00028
R_{ct} (Ω)	50.67	51.72	48.73	52.38	64.89	132.7	193.3	43.28
CPE-T ($S \cdot s^n$)	5.56E-08	8.16E-08	1.44E-07	2.04E-07	2.12E-07	2.11E-06	1.26E-05	1.47E-08
CPE-P	1.178	1.143	1.115	0.98	1.043	0.816	0.774	1.356
W_o-R	445.5	335.8	49.23	380.2	331.6	418.2	674.2	74.01
W_o-T ($S \cdot s^n$)	24.54	20.82	1.145	5.81	2.105	1.236	0.263	2.805
W_o-P	0.34	0.33	0.19	0.35	0.35	0.36	0.24	0.18

Chi-squared	0.00036886	0.00020264	0.00015583	0.00030302	0.00075162	0.0085971	0.019443	0.003638

These materials' energy storage/release process is accompanied by reversible color changes (charging/discharging) during the electrochemical redox reactions. This feature is promising for developing bi-functional colorimetric energy storage devices. The transmittance spectrum of WO_3 films is measured at different potentials, with the observed color-switching gradually from transparent to dark blue. The results show an excellent EC performance, as shown in Fig. 3a, which can be easily seen with naked eyes. The dynamic color changing process is demonstrated in VideoS1. To further evaluate the charge storage/release dynamics and its dependence on potentials and *f*, a 3D Bode plot is presented for the *f* range of 1.2 to 0.1 Hz in Fig. 3b. The low *f* can slow down the redox processes and allow the maximum Li^+ insertion/de-insertion, giving rise to a high capacitance. As *f* increases, the capacitance quickly falls off, suggesting that the redox processes are prominent within this *f* range. Based on prior reports by Simon et al.[17], 3D Bode representations provide a complete experimental understanding of the complex interplay of capacitance as a function of *f*, potential, and even the electrolyte compositions. For electrical double-layer type, the capacitance will stay constant across the potential window at any given *f*, demonstrating a rectangular waterfall shape[18]. For the pseudo capacitor behavior at low *f*, the capacitance increases with potential step by step and reaches its peak value. The capacitance rapidly falls off after the potential is reversed when the potential exceeds 0.15 V (*vs.* Ag/AgCl). This observation reveals that WO_3 charge storage dynamics at low *f* correspond to redox processes operating at various potentials. High capacitance above 80 mF/cm^2 is achieved at a low *f* of 0.1 Hz under the potential of -0.5 V in coloration. The electrochemical redox reactions cause the pseudocapacitive charge storage/release of WO_3 thin solid films and the coloration/bleaching behavior. The charging/discharging process and the reduction/oxidation reactions are also demonstrated by WO_3 thin films. To further illustrate the EC charge storage mechanism, the $Li^{+,}$ and e^- dual injection/extraction model is constructed in Fig. 3c. The movement of the charges causes the decrease/increase of the valence states of tungsten ions, accompanied by coloration/bleaching (blue/transparent) when the potential is applied.

Fig. 4a shows the typical CV for amorphous WO_3 thin solid films at various scan rates from 150 to 20 mV/s within a narrow electrochemical window. The area enclosed by the curves represents the total stored charges arising from both faradaic (diffusion-controlled) and non-faradaic (electrical double layer capacitive) processes. In the coloration process, the continuously increasing faradaic current indicates Li^+ and e^- dual insertion behavior, accompanied by the reduction of the WO_3. The broad anodic peak represents the Li^+ and e^- extraction accompanied by the reversible oxidation and thus the bleaching phenomenon. The pseudocapacitive effects are characterized by analyzing the CV data at various sweep rates based on the power-law $i = av^b$[19]. In particular, $b = 1.0$ is indicative of a capacitive process due to the capacitive current being directly proportional to the sweep rates, independent of the diffusion-redox process. For $b = 0.5$, the current is proportional to the square root of v, identifying a semi-infinite diffusion. The linearized relationship of data extracted from the anodic peak current and low sweep rates gives the b-value around 0.5, indicating the current is predominantly Li^+ insertion/de-insertion faradaic current. A relatively slow scan rate is favorable for the Li^+ insertion/de-insertion process.

To further examine the charge storage dynamics, the total current at each potential can be expressed as two processes: the surface capacitive and diffusion-controlled parts: $i(V) = k_1v+k_2v^{1/2}$ or $i(V)/v^{1/2} = k_1v^{1/2}+k_2$. By determining k_1 and k_2, we can obtain the current fraction at each potential and then quantify their contributions to the total charge storage. The linear relationship of $i(V)/v^{1/2}$ *vs.* $v^{1/2}$ enables us to obtain the k_1 and k_2 from the slope and the y-axis intercept, respectively, at every single potential [2]. We used the Python coding to determine the k_1 values, and only the good fit that resulted in a linear fit coefficient greater than 0.95 was taken into account. In Fig. 4c, the capacitive current shown as the shaded area is compared with the total experimental current at the sweep rate of 30 mV/s. The panel d in Fig. 4 shows the relative contributions of the surface capacitive effects to the total charge storage. At scan rates lower than 40 mV/s, the Li^+ diffusion process is dominant over the surface capacitive behavior and follows the calculated b-values given in Fig. 4b. As the scan rate increases, the capacitive current catches up and takes over the response. The disagreement between the two different charge storage mechanisms becomes very pronounced at higher scan rates (as high as 100 mV/s) and is closely associated with the capacitors' rapid charge/discharge characteristics.

Surface Imaging

There have been several advances in the realm of 3D surface imaging technologies that allow further investigations of the complexity of the WO_3 EC thin solid films. The method of 3D surface imaging allows mapping of the surface of interest in the 3D space[20]. Fig. 5 shows the surface image captured using Optical Profilm 3D. We determine the thickness of the film by measuring the step height between the as-deposited WO_3 and the ITO/glass substrate, as shown in Fig. 5a. The ITO/Glass was partially masked during the sample preparation to provide a stepped region of comparison. Once the deposition was completed, the mask was removed for step height analysis. The step is shown using the cross-sectional diagram, and the height scale for the height is provided in the top left image. The difference between the film and the substrate is 480 nm. Fig. 5b shows a similar analysis of the regions between the lithiation (colored) and de-lithiation (bleached) states. A non-negligible thickness difference is expected due to the lithiation process. Spatial analysis shows the presence of a border between lithiated and un-lithiated areas. The active Li^+ cations cause the boundary between the blue and transparent areas. We estimated that the Li^+ incorporation brings approximately 3.12% volume expansion of the WO_3 thin film.

Conclusion

EC pseudocapacitive charge storage in transition-metal oxide WO_3 thin films has been demonstrated and investigated. A high areal charge density of 100 mC/cm^2 and a capacitance of 80 mF/cm^2 were achieved under the MSCA and EIS low-*f* diffusion operations. Moreover, diffusion-controlled and surface capacitive processes were separated based on power law. The color-switching enabled the direct visualization of charge statuses, with wide optical contrast of over 90%. Pseudocapacitive transition-metal oxides combine the fast response, high energy density, visual indication, and potential for miniaturization, and pave the way for developing novel charge storage materials and devices.

Acknowledgments

This work is partially supported by DOE-NNSA funded MSIPP program Advanced Sensors Technologies for Applications in Electrical Engineering-Research and Innovation eXcellence Consortium (ASTERIX) under award number 800012972.

References

1. Z. Luo, L. Liu, X. Yang, X. Luo, P. Bi, Z. Fu, A. Pang, W. Li, and Y. Yi, *ACS App. Mater. Interface*, **12**(35), 39098 (2020).

2. L. Liu, Q. Zhang, K. Du, Z. He, T. Wang, Y. Yi, M. Wang, X. Zhong, G. Dong, and X. Diao, *J. Mater. Chem. A*, **7**(40), 23028 (2019).
3. H. Li, J. Li, C. Hou, D. Ho, Q. Zhang, Y. Li, and H. Wang, *Adv. Mater. Technol.* **2**, 1700047 (2017).
4. S. Lin, X. Bai, H. Wang, H. Wang, J. Song, K. Huang, C. Wang, N. Wang, B. Li, M. Lei, and H. Wu, *Adv. Mater.*, **29**, 1703238 (2017).
5. Z. Liu, H. I. Wang, A. Narita, Q. Chen, Z. Mics, D. Turchinovich, M. Kläui, M. Bonn, and K. Müllen, *J. Am. Chem. Soc.*, **139**, 9443 (2017).
6. T. Y. Yun, X. Li, S. H. Kim, and H. C. Moon, *ACS Appl. Mater. Interfaces*, **10**, 43993 (2018).
7. P. Yang, P. Sun, and W. Mai, *Mater. Today*, **19**, 394 (2016).
8. L. Zhang, M. Liao, L. Bao, X. Sun, and H. Peng, *Small Methods*, **1**, 1700211 (2017).
9. J. Li, A. Levitt, N. Kurra, K. Juan, N. Noriega, X. Xiao, X. Wang, H. Wang, H. N. Alshareef, and Y. Gogotsi, *Energy Storage Mater*., **20**, 455 (2019).
10. D. Dong, J. Robichaud, and Y. Djaoued, *Canadian J. Chem.*, **99**(6), 549 (2021).
11. J. Wang, J. Polleux, J. Lim, and B. Dunn, *J. Phys. Chem. C*, **111**(40), 14925 (2007).
12. M. Sathiy, A. S. Prakash, K. Ramesha, J. M. Tarascon, and A. K. Shukla, *J. Am. Chem. Soc.*, **133**, 16291 (2011).
13. T. M. Dinh, A. Achour, S. Vizireanu, G. Dinescu, L.Nistor, K. Armstrong, D. Guay, and D. Pech, *Nano Energy*, **10**, 288 (2014).
14. S. M. Park and J. S. Yoo, *Analytical Chemistry*, **75**(21), 455 (2003).
15. W. Liu, H. Yi, Q. Zheng, X. Li, and H. Zhang, *J. Mater. Chem. A*, **5**, 10928 (2017).
16. K. Li, X. Wang, X. Wang, M. Liang, V. Nicolosi, Y. Xu, and Y. Gogotsi, *Nano Energy*, **75**, 104971 (2020).
17. P. L. Taberna, P. Simon, and J. F. Fauvarque, *J. Electrochem. Soc.*, **150**(3), A292 (2003).
18. N. Kurra, S. Uzun, G. Valurouthu, and Y. Gogotsi, *Energy Stor. Mater. 39*, 347 (2021).
19. Q. Wei, R. H. DeBlock, D. M. Butts, C. Choi, and B. Dunn, *Energy Environ. Mater.*, **3**, 221 (2020).
20. J. Geng, *Adv. Opt. Photon*, **3**, 128 (2011).

Figures

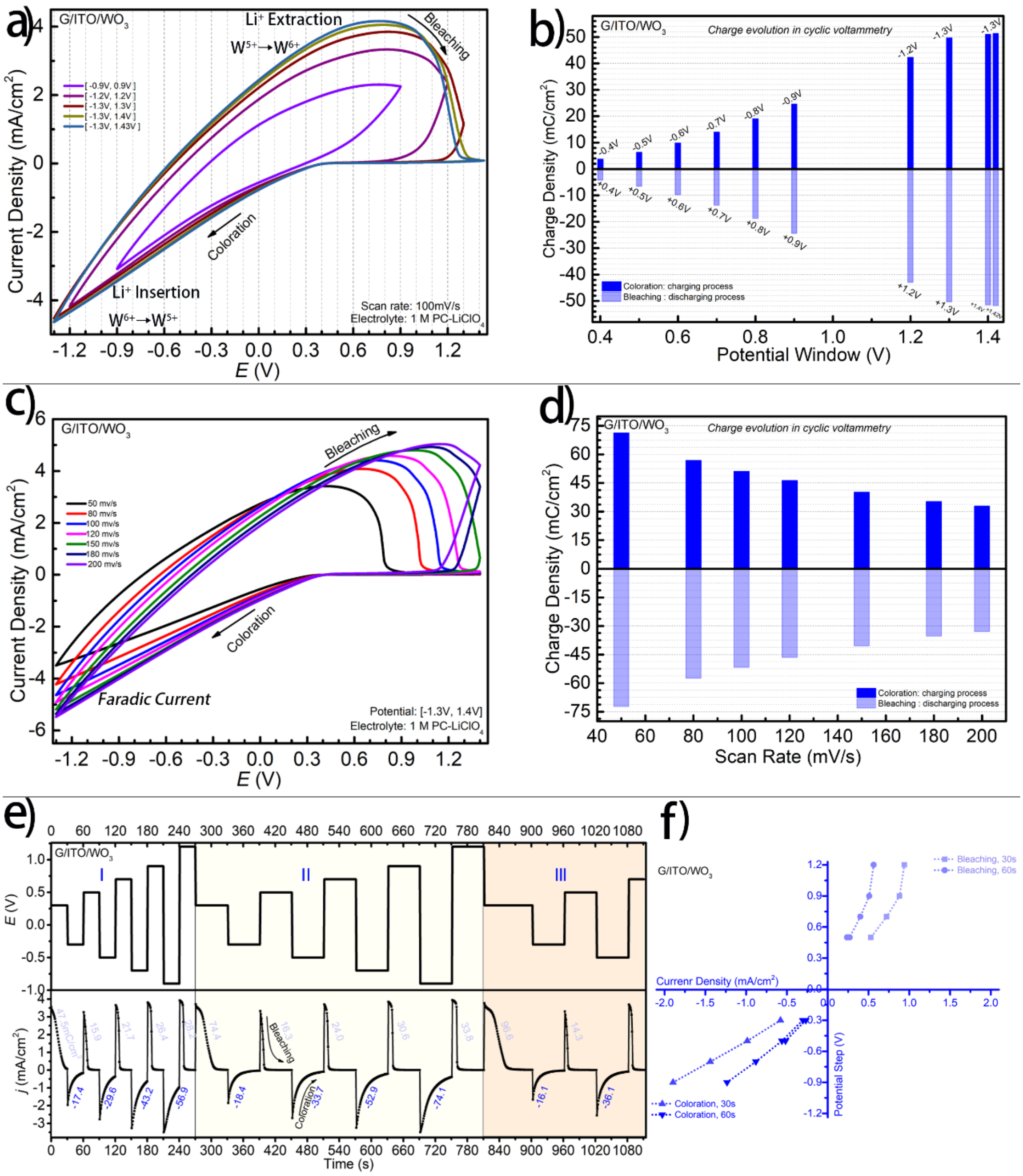

Fig. 1. Electrochemical kinetics of WO_3 electrode. (a) CV curves at various potential windows and (b) corresponding charge capacities. (c) CV curves at different scan rates and (d) relevant charge capacities. (e) Multi-step CA curves vary with potentials and duration time, and (f) average current densities. (Active area: 2.5 cm×0.7 cm)

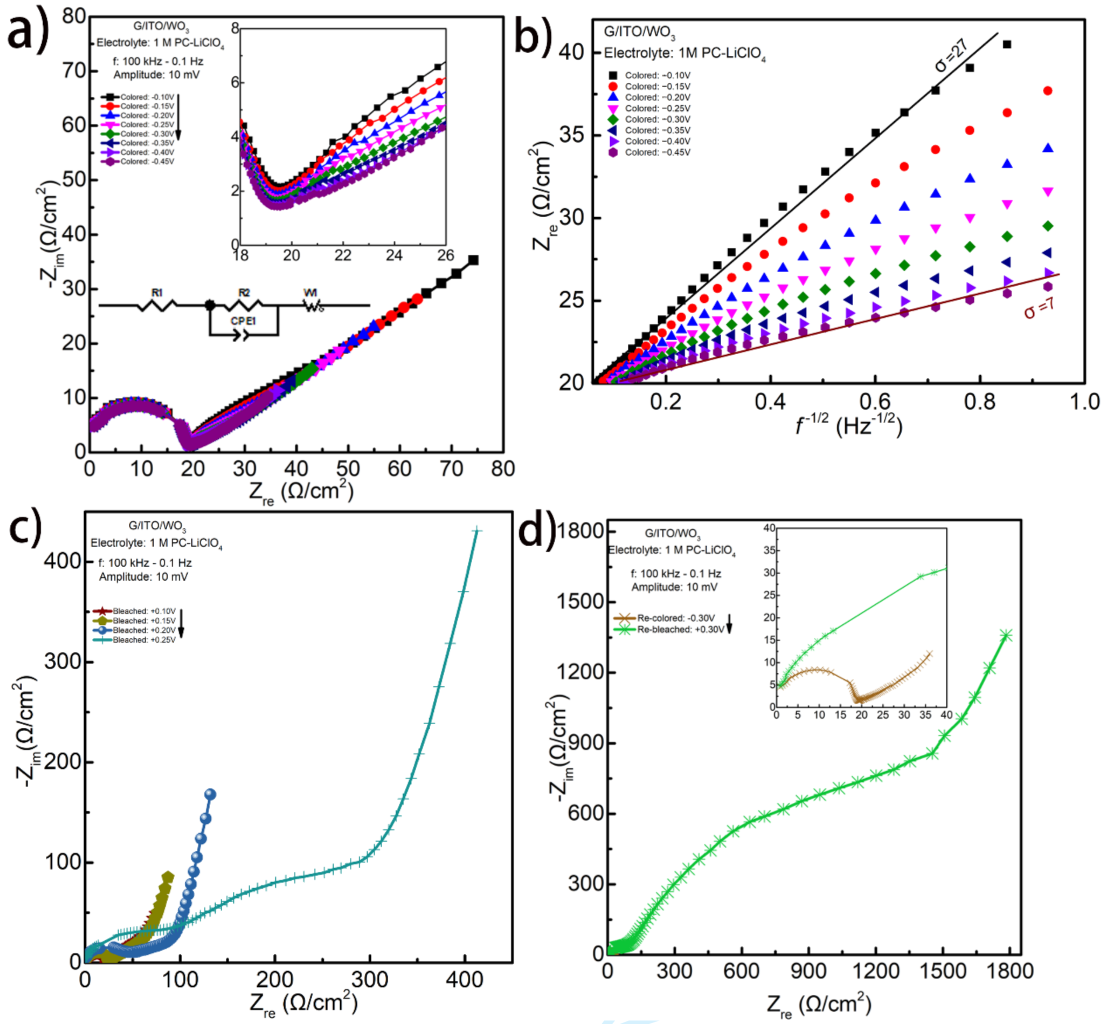

Fig. 2. EIS data and analysis for the WO_3 electrode. Real *vs.* negative imaginary impedance for the WO_3 thin solid film measured in a 1 M PC-$LiClO_4$ electrolyte: (a)/(c)/(d) at colored/bleached/(re-colored/re-bleached) states, and (b) Linear fit of Z_{re} against $f^{-1/2}$. Insets are enlargements of the high-*f* EIS region and the equivalent-circuit model.

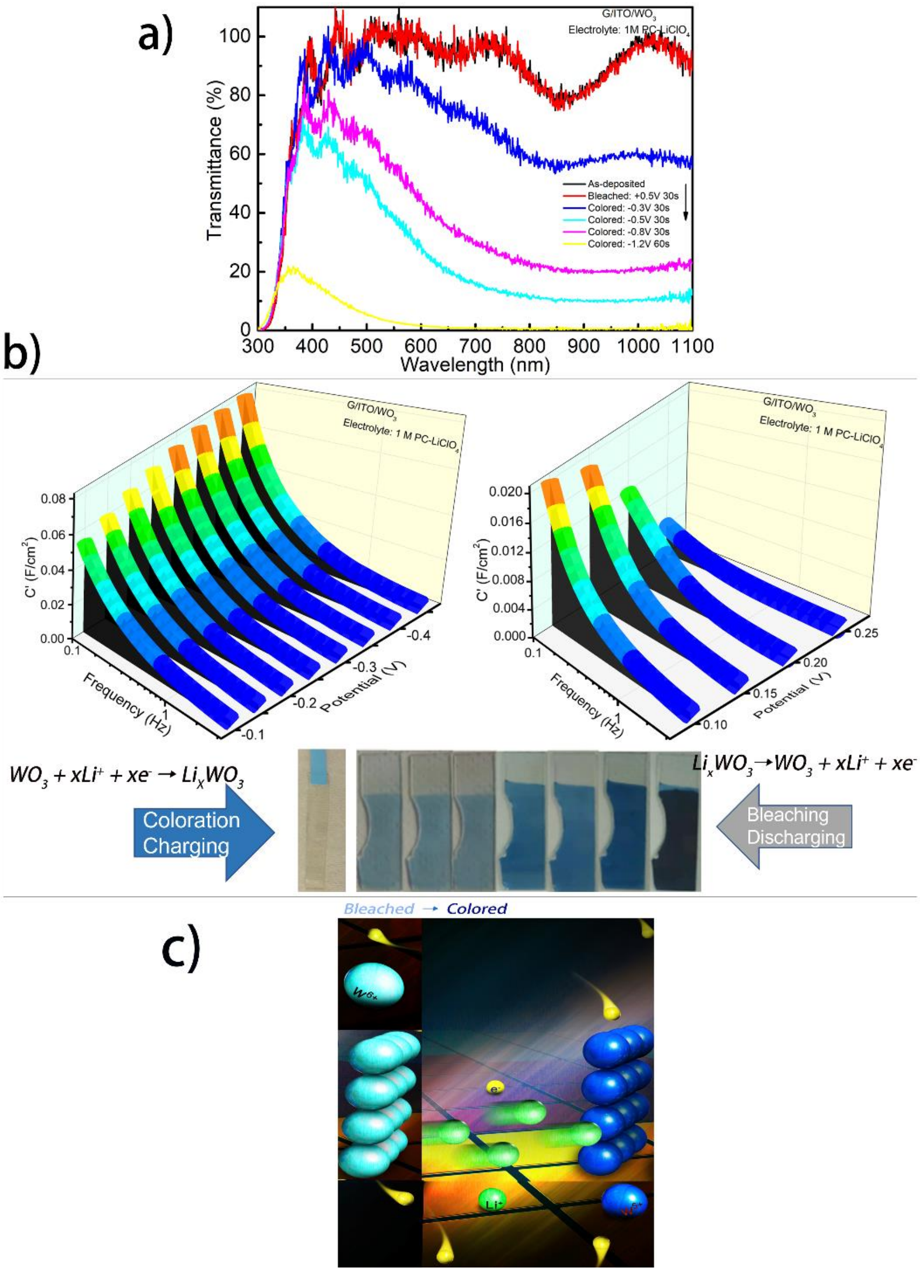

Fig. 3. Visualized energy storage status of EC WO_3 thin solid films. (a) Optical transmittance of colored/bleached WO_3 varying with potentials. (b) The 3D Bode plot representations of the real capacitance C' *vs*. *f vs*. potential and optical images at different charging/discharging states with potentials ranging from 0 to -1.2 V. (c) Electrochemical ion/electron dual injection/extraction mechanism.

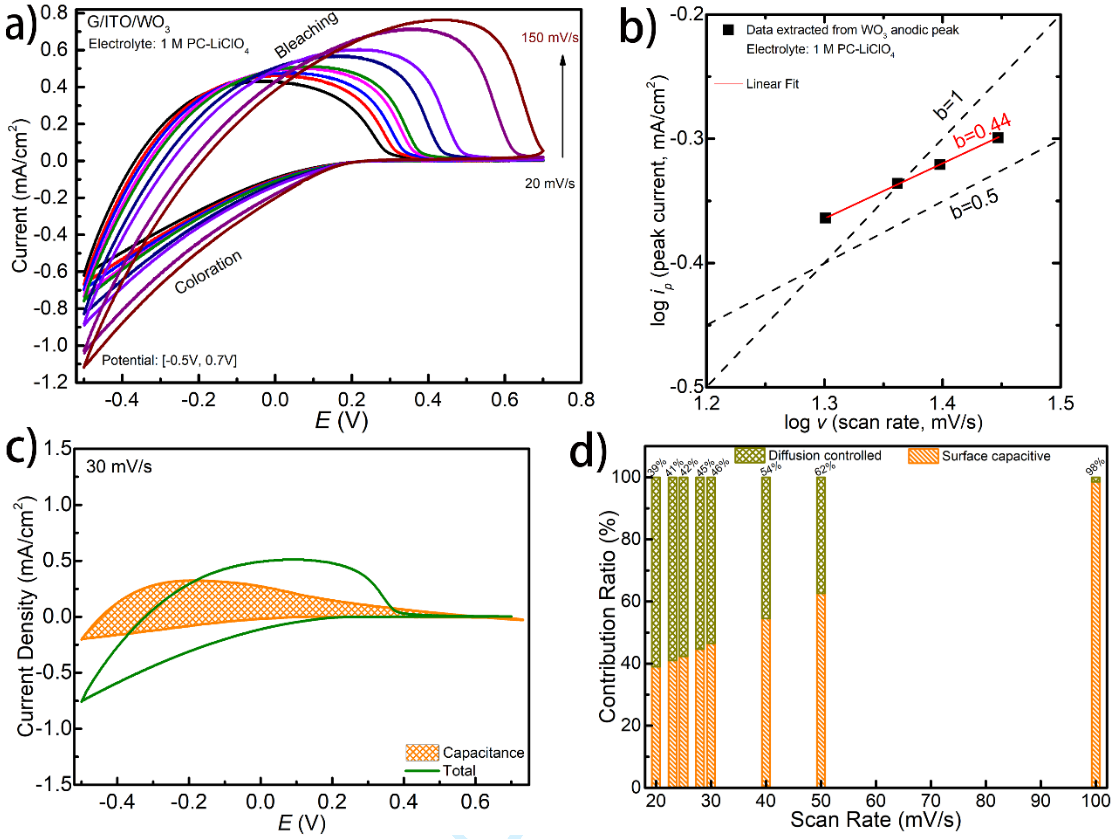

Fig. 4. Pseudo capacitive charge storage of the EC WO_3. (a) CV curves at continuously decreasing scan rates: 150, 100, 50, 40, 30, 28, 25, 23 and 20 mV/s (Active area: 3.5 cm * 0.7 cm). (b) Linear fitting of log i_p *vs.* log v. (c) CV curves at 30 mV/s illustrating the surface capacitance contribution (shadow area) to the total. (d) Percentage of diffusion-controlled and surface capacitive behavior varying with scan rate.

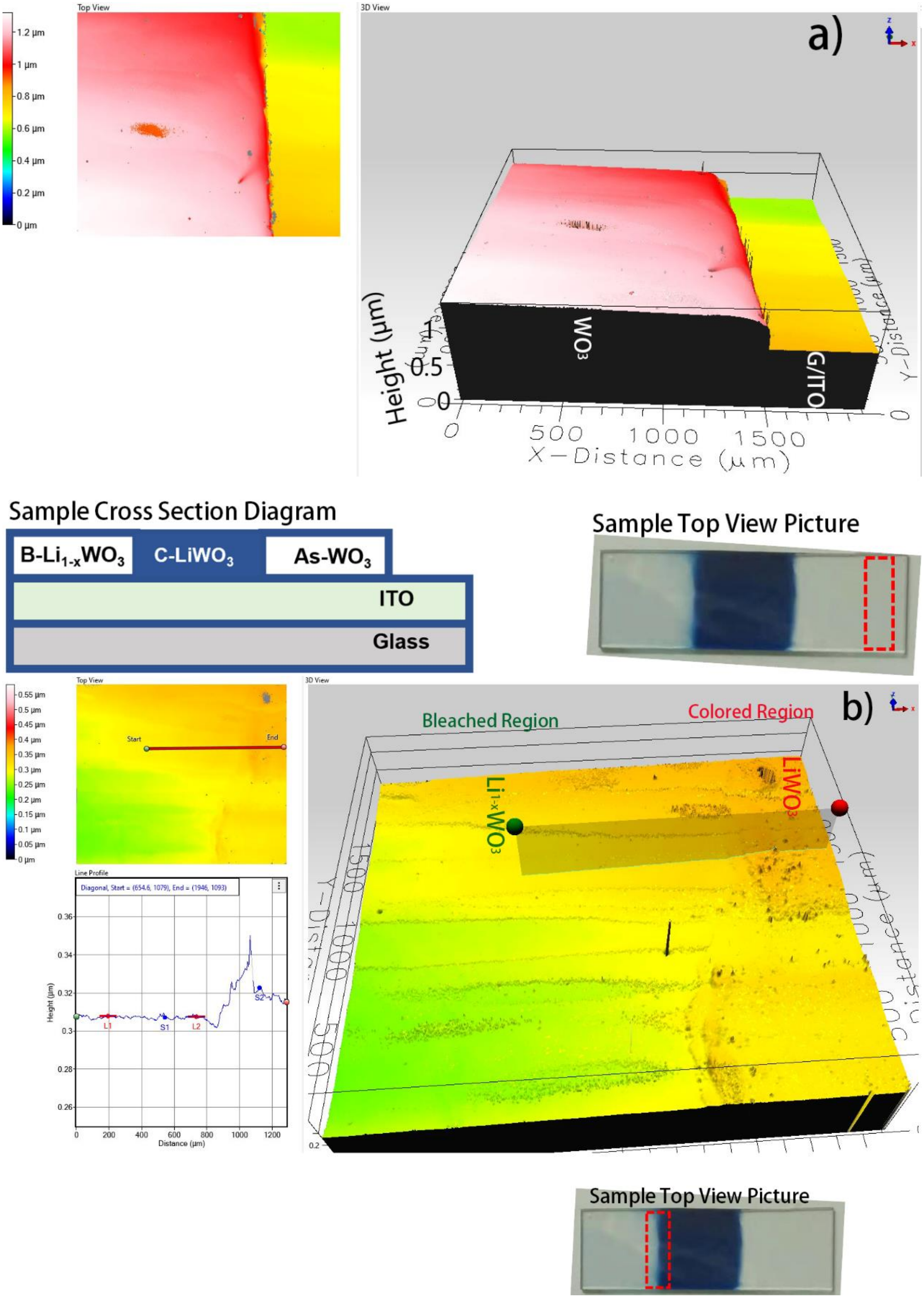

Fig. 5. Surface Imaging by Optical Profilm 3D. (a) Thickness measurement and the diagram/image of bleached-colored-initial WO_3 sample. (b) Spatial analysis at the boundary of the de-lithiation (bleached) and lithiation (colored) regions.